# Surface Sensitivity in Lithium-Doping of MgO: A Density Functional Theory Study with Correction for on-Site Coulomb Interactions

**David O. Scanlon, Aron Walsh,† Benjamin J. Morgan, Michael Nolan, Joanne Fearon, and Graeme W. Watson***

*School of Chemistry, University Of Dublin, Trinity College, Dublin 2, Ireland*

*Received: January 10, 2007; In Final Form: March 29, 2007*

Catalytic conversion of methane to higher hydrocarbons takes place on lithium-doped MgO. To date, investigations of the Li-doping process have been confined to the bulk and the (100) surface. In this paper, we describe an investigation of the surface dependence of Li-doping of MgO through an in-depth study of the (100), (110), and (111) low index surfaces using density functional theory with correction for on-site Coulomb interactions (DFT+*U*). Three competing defect configurations were investigated on each of the surfaces; substitution of Li for Mg with the formation of a compensating oxygen hole state, substitution of Li for Mg with the addition of a Li surface interstitial and the clustering of two Li ions with the formation of a neutral [$Li'_{Mg}$ $V_O^{\bullet\bullet}$ $Li'_{Mg}$] oxygen vacancy. Our results demonstrate that the energetics associated with the Li-doping of MgO are strongly surface dependent. On the (100) surface, there is an energy cost associated with Li-doping, whereas on the (110) and (111) surfaces Li-doping is energetically favored. The implications of the results for the catalytic activity of the different surface terminations of MgO are discussed.

## 1. Introduction

Methane is a highly abundant natural resource, and the identification of catalysts that can transform methane into other desirable products is a major research aim within the petrochemical industry. Oxidative coupling of methane to $C_2$ hydrocarbons enjoyed research popularity in the late 1980s and early 1990s with the discovery that Li-doped magnesium oxide catalyzes the coupling of methane[1]

$$2CH_4 + {}^1/_2O_2 \rightarrow C_2H_6 + H_2O$$

$$2CH_4 + O_2 \rightarrow C_2H_4 + 2H_2O$$

This catalyst, when operated at high temperatures, was found to produce a significant fraction of $C_2$ hydrocarbons (ethane and ethene) with up to 73% selectivity at 7% Li-doping. An industrial process based on such a catalyst could provide significant savings over traditional methods of conversion via synthesis gas.

The most commonly accepted reaction mechanism for methane coupling over Li-doped MgO begins with the extraction of a hydrogen atom from methane to form a methyl radical, which then reacts further with other such radicals present in the gas phase.[2] Wu et al.[3] have conducted a high-resolution electron energy loss spectroscopy study of Li-doped MgO and have noted that at temperatures greater than 1100 K a new loss feature at 1.6 eV is observed. This is attributed to the formation of $O_O^{\bullet}$ electron holes, situated at the surface, which are the proposed reactive sites for the extraction of hydrogen radicals from $CH_4$. The presence of a trapped hole on a single oxygen atom has been confirmed by electron paramagnetic resonance[4−8] and through reaction with NO.[1,4] Electron spin resonance and electron nuclear double resonance (ENDOR) techniques have also been employed in detailed studies of Li-doped MgO defect centers, allowing both an examination of the geometry of the defect center and the nature of the electronic hole to be determined.[9−11] The presence of hyperfine components in the ENDOR spectrum was also attributed to the formation of a [$Li'_{Mg}O_O^{\bullet}$] center with the electronic hole localized on a single oxygen ion.[9] Determination of the geometry of the defect center is also possible by decomposition of the magnetic hyperfine interaction, although the calculated Li−O distance depends on the radial extent of the O 2p orbital function used in the analysis. On the application of a number of models, Li−O distances in the range 2.37−2.59 Å were found,[9] all of which are substantially longer than the bulk Mg−O distance of 2.11 Å and the Li−O distance of 2.00 Å in $Li_2O$.

Computational methods have been used extensively to study oxygen hole formation on Li-doped MgO.[12−18] Cluster model studies using unrestricted Hartree−Fock (UHF) have been presented by Zuo et al.[12] and Lintuluoto and Nakamura.[13] The embedded cluster study of Zuo et al. found a contraction of 21% of the Li−O distance in the defect center, compared to a bulk MgO bond length,[12] which is strongly at variance with experimental findings that the Li−O distance is elongated.[5−8] Lintuluoto and Nakamura considered bare cluster models of the Li-doped (100) MgO surface and observed a single increased Li−O interatomic distance of 2.58 Å, which is consistent with experiment. Analysis of atomic charges and spin densities showed localization of the hole on the oxygen atom with the elongated Li−O bond, again showing consistency with experimental results.[5−8] Oxygen hole formation has also been studied using periodic UHF.[14−16] When the [$Li'_{Mg}O_O^{\bullet}$] defect is modeled using periodic UHF, one Li−O distance is elongated to 2.44 Å. The UHF band structure shows that the unpaired electron occupies an O 2p orbital that is lower in energy than

* To whom correspondence should be addressed. E-mail: watsong@tcd.ie. Tel: +353 1 8961357.

† Current Address: National Renewable Energy Laboratory, Golden, Colorado 80401.

10.1021/jp070200y CCC: $37.00 
Published on Web 05/11/2007

the onset of the valence band. The corresponding unoccupied O 2p orbital appears as a gap state lying between the valence band and the conduction band. Both the elongated bond length and spin localization are consistent with experimental observations.[5−8]

In the UHF study by Dovesi et al.,[16] the authors additionally reported a density functional theory (DFT) calculation of the electronic structure. However, they did not succeed in localizing the unpaired electron, which was described by DFT as being distributed over the six oxygens neighboring the Li-dopant. Later DFT studies have displayed vastly different findings to UHF.[17,18] Yang et al.[17] investigated electronic hole formation on the (100) surface within the local density approximation of DFT, while Dash and Gillan[18] investigated the same surface within the generalized gradient approximation (GGA), starting from a high-symmetry geometry. In both studies, the Li−O interatomic distances were found to be equal, and the electronic density of states (EDOS) calculated for the Li-doped surface shows the valence band crossing the Fermi level with no defect state produced in the energy gap. Nolan and Watson have also conducted a GGA study of this defective surface and have shown that a symmetry-broken starting geometry also results in a symmetric solution, with the electronic hole delocalised over several O centers and uniform Li−O distances.[19] These results show that uncorrected DFT gives a description of the defect geometry and electronic structure that is inconsistent with both the calculated UHF results and with experimental data.

The problem of describing localized O 2p holes in doped metal oxides with DFT is rather widespread.[20−26] It has been extensively discussed for Al-doping of silica[20,24,25] where the UHF results are consistent with experiment and the DFT results are not. Further examples include cuprate semiconductors ($La_2CuO_4$)[21] as well as $SrCoO_3$[22] and $LaFeO_3$[23,26]. The origin of this problem lies in the failure of DFT to cancel the electron self-interaction. One approach to compensate for this is to use DFT corrected for on-site Coulomb interactions for strongly correlated systems (DFT+*U*).[27−30] In this context, Nolan and Watson have also studied the electronic structure and energetics of hole formation for the Li-doped (100) MgO surface using DFT+*U*,[19] which gave results in agreement with both experimental data and previous UHF calculations in contrast to the uncorrected DFT calculations described above.

In the present paper, we apply DFT+*U* to study the surface dependence of Li-doping of MgO. The difference in charge between Mg and Li requires the formation of a charge-compensating defect. There are a number of ways in which this compensation could take place. The direct substitution of Li for Mg with electronic compensation, in the form of an oxygen hole state, produces a catalytically active $[Li'_{Mg}O^{\bullet}_{O}]$ defect as previously discussed and which previous studies have considered

$$Li_2O + \frac{1}{2}O_2 \rightarrow 2[Li'_{Mg}O^{\bullet}_{O}]$$

However, there are alternative, competing, charge-compensating mechanisms. Pairs of Mg atoms can be replaced with Li in a clustered configuration next to an oxygen vacancy. In stoichiometric MgO, a neutral oxygen vacancy leaves behind two electrons. However, in a clustered $[Li'_{Mg}\ V^{\bullet\bullet}_{O}\ Li'_{Mg}]$ defect, because each Li-dopant ion has a formal charge of +1 in comparison with the +2 of Mg, a neutral oxygen vacancy contains no extra electrons and consequently the defect center is likely to be catalytically inactive

$$Li_2O \rightarrow 2Li'_{Mg} + V^{\bullet\bullet}_{O} + O_O$$

Another alternative compensating configuration is the substitution of Li for Mg accompanied by the introduction of an additional interstitial Li atom. The addition of the Li interstitial on the Li-doped surface produces another defect center, which is potentially catalytically inactive

$$Li_2O \rightarrow Li'_{Mg} + Li^{\bullet}_{i} + O_O$$

The latter two mechanisms for Li incorporation can also be thought of as solution mechanisms. In the following work, we present a study of Li-doping of MgO, examining the different charge-compensating mechanisms and their dependence on the (100), (110) and (111) surfaces.

## 2. Methods

Calculations of equilibrium geometry and electronic structure for the systems of interest were performed using the periodic DFT code, VASP,[31,32] with valence electrons described within a plane wave basis set. The interaction between the core (Mg: [Be] and O: [He]) and valence electrons is handled by the projector-augmented wave method,[33] which approaches the accuracy of an all electron calculation while maintaining the computational efficiency of a standard pseudopotential. For Li, all electrons are explicitly treated as valence. The Perdew−Burke−Ernzerhof[34] gradient corrected exchange−correlation functional is applied. The calculations performed were fully spin polarized to be able to describe the unpaired electron produced on doping Mg(II)O with a single Li(I).

DFT+*U* has previously been employed to correct for on-site Coulomb interactions in strongly correlated systems[28,35,36] and is applied in all the calculations. In this instance, the term strongly correlated refers to the physics terminology of strong Coulomb interactions resulting in localized electronic states. In HF, the Coulomb interaction is correctly described with the exact exchange term cancelling the unphysical electron self-interaction. In DFT however, exchange is only approximated, so the self-interaction is not correctly cancelled. This results in the self-interaction error, which causes the poor description of strongly correlated systems.[20] DFT+*U* introduces a HF-like term to cancel this self-interaction error. This methodology is generally applicable to cases where DFT fails to give the correct localized solution. The value of *U*, which is applied to the oxygen p orbitals and which is used in all the work described herein, is 7 eV, which has previously been shown to be suitable for the description of the (100) MgO surface with a $[Li'_{Mg}O^{\bullet}_{O}]$ defect center,[26] giving atomic and electronic structures that are consistent with both experimental data and earlier UHF results.

To calculate equilibrium lattice parameters for the chosen model, structural optimizations of bulk MgO were performed at a series of volumes, allowing the atomic positions, lattice vectors, and cell angles to relax while the total volume was held constant. The resulting energy volume curves were fitted to the Murnaghan equation of state[37] to obtain the equilibrium bulk cell volume, which was then used in generating the surfaces of interest. This approach was taken to avoid the problems of Pulay stress and changes in basis set that accompany volume changes in plane wave calculations.

To describe surfaces within three-dimensional periodic boundary conditions, the slab method was employed. Within this approach, the model system was constructed as a $2 \times 2$ supercell two-dimensional slab of finite thickness, periodically repeated in the three Cartesian dimensions. The (100), (110), and (111) MgO surfaces were cleaved from bulk MgO configurations using METADISE.[38] The periodic slabs are separated by a

vacuum gap in the direction perpendicular to the surface planes, which is large enough to remove spurious slab−slab interactions. A vacuum thickness of 15 Å between periodic slab images was applied in all calculations.

Each surface was tested for convergence of surface energy against slab thickness. This resulted in thicknesses of 12.12 Å (6 atomic layers) for the (100) surface, 11.90 Å (6 atomic layers) for the (110) surface, and 12.22 Å (13 atomic layers) for the (111) surface. A $2 \times 2 \times 1$ *k*-point sampling mesh and a plane wave energy cutoff of 500 eV were also used for each surface to ensure suitable energy convergence. The modifications made to the atomic structure in preparing defective systems were performed identically on both sides of the slab to ensure that the slab dipole moment perpendicular to the surface was zero.

MgO has the B1 rock salt structure, and consequently the (100) and (110) surfaces are defined by Tasker[39] as type 1 surfaces for which the surface layer is a charge neutral array of equal numbers of cations and anions. Conversely, the (111) surface is of type 3 being composed of alternating charged planes that give rise to a dipole perpendicular to the surface. As a consequence, the bulk crystal can be cleaved to form a (111) surface terminated with either cations (Mg) or anions (O); we have considered both surfaces in this work. To remove the large dipole perpendicular to the surface that would otherwise be present, half the exposed atoms uppermost on one (111) surface were transferred to the opposite side of the slab in a process similar to that employed in other type 3 oxide surface calculations.[40] Previous DFT work has shown such a formation of (100) microfacetting to be the most stable reconstruction of the MgO (111) surface.[41] For an unmodified (111) surface, the ions that make up the uppermost surface layer each sit at the apex of a trigonal bipyramid, and have a coordination environment with trigonal symmetry. Removing $<1\bar{1}1>$ rows of ions from one side of the slab and replacing them on the opposite side lowers the symmetry of the surface sites, making the three counterions in the subsurface layer nonequivalent. Two remain equivalent to each other and occupy five-coordinate bridging sites, each coordinated to two surface atoms; the third lies on the other side of the surface ion in a nonbridging four-coordinate site being coordinated to a single surface ion. In what follows, these sites will be denoted $X_b$ and $X_{nb}$, where X is Mg in the case of an oxygen-terminated surface, and O in the case of a magnesium-terminated surface. For each surface considered, a full ionic relaxation was performed after construction to find an equilibrium energy and geometry. The structures were deemed to be converged when the forces on all the ions were less than 0.01 eV $Å^{-1}$.

DFT+*U* calculations using the same calculation parameters and convergence criteria as described above were also performed on $Li_2O$ and molecular oxygen, so that consistent energies could be obtained for use in the defect formation energy calculations presented below.

## 3. Results

**3.1. Pure Surfaces.** The relaxed surface energies for the stoichiometric surfaces are 0.91 J $m^{-2}$ for the (100) surface, 2.31 J $m^{-2}$ for the (110) surface, 3.44 J $m^{-2}$ for the Mg-terminated (111) surface, and 3.58 J $m^{-2}$ for the O-terminated (111) surface. The (100) surface is by far the most energetically stable stoichiometric surface, as expected for rock salt-structured metal oxides.

The relaxed (100)-terminated surface results in a nearest neighbor Mg−O interatomic distance of 2.11 Å on the surface, which is relatively unperturbed from the bulk. For the (110) surface, two pairs of Mg−O atoms are relaxed to interatomic distances of 2.11 Å and 2.02 Å, respectively. The Mg-terminated (111) surface distorts strongly upon relaxation and results in three-coordinate surface cation sites with two Mg−O interatomic distances of 1.88 Å and one of 1.86 Å. For the O-terminated (111) surface, there are two unique types of cation site. The surface nonbridging site is four-coordinate with two Mg−O distances of 2.20 Å, one of 1.99 Å, and one of 1.86 Å. The corresponding bridging cation site is five-coordinate with two oxygens at a distance of 2.28 Å, two at 1.88 Å, and one at 2.19 Å. These equilibrium geometries are in good agreement with previous MgO surface studies.[41−43]

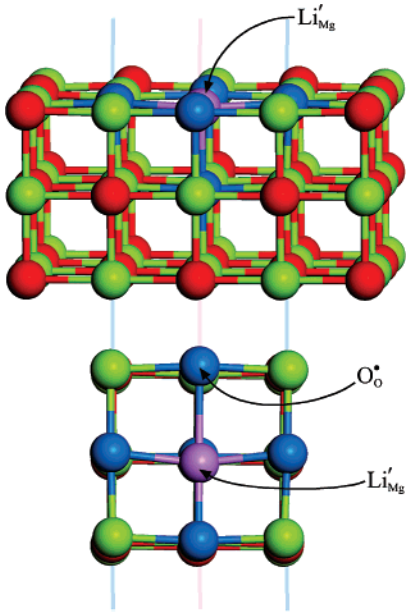


**Figure 1.** The relaxed DFT+*U* geometry of Li-doped (100) MgO with $[Li'_{Mg}O^{\bullet}_{O}]$ defect. Side view (upper panel) and top view (lower panel) of the geometry around the Li-dopant. The Mg atoms are colored green, Li atoms colored purple, O atoms coordinated to the Li colored blue, and all other oxygen atoms colored red.

**3.2. Lithium-Doping with Oxygen Hole Electronic Compensation.** To construct the Li-doped MgO surfaces with electronic compensation in the form of an oxygen hole, a surface Mg atom was replaced with a Li atom. The symmetry of the defect site was then lowered by moving one oxygen adjacent to the Li-dopant off its lattice site by extending the relevant Li−O bond length. This breaking of symmetry has been shown to be necessary to achieve relaxation to a geometry with a correctly localized electronic structure.[19]

The DFT+*U* relaxed geometry for the $[Li'_{Mg}O^{\bullet}_{O}]$ (100) structure, with the dopant in a surface site, is shown in Figure 1. There is a single elongated Li−O distance of 2.38 Å, compared to the pure Mg−O surface distance of 2.11 Å, and a corresponding shortened Li−O distance of 1.92 Å, both of which are colinear along the <010> direction. The remaining interatomic distances in the surface layer are less strongly perturbed. The geometry qualitatively agrees with previously published experimental and UHF data[5−8,13−16] and our previous DFT+*U* calculations, in which a 5-layer slab of the (100) surface was used.[19]

When doping the (110) surface, one of the Mg atoms in an upper ridge was chosen as the substitution site. The subsequently relaxed geometry is shown in Figure 2. A single Li−O distance is elongated to 2.43 Å, compared with 2.22 Å on the pure (110) surface.

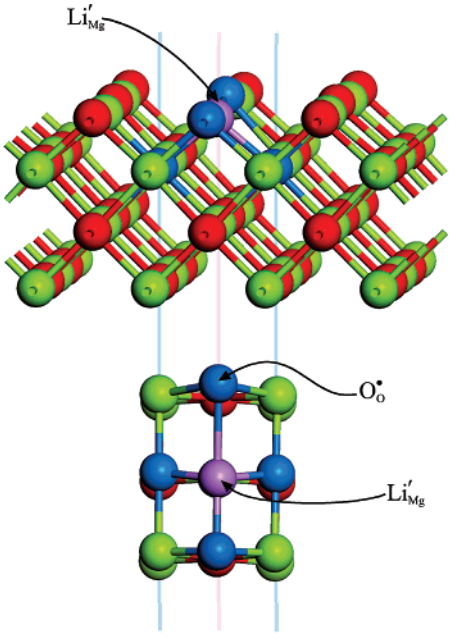


**Figure 2.** The relaxed DFT+*U* geometry of Li-doped (100) MgO with $[Li'_{Mg}O^{\bullet}_{O}]$ defect. Side view (upper panel) and top view (lower panel) of the geometry around the Li-dopant.

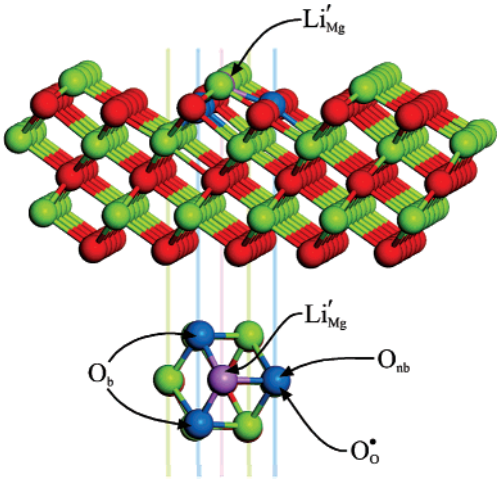


**Figure 3.** The relaxed geometry of the Li-doped (111) Mg-terminated MgO surface with $[Li'_{Mg}O^{\bullet}_{O}]$ defect, indicating the bridging and nonbridging nearest-neighbor sites. Side view (upper panel) and top view (lower panel) of the geometry around the Li-dopant.

For the Mg-terminated (111) surface, again a Mg ion at the surface was replaced with a Li-dopant. The oxygen atoms coordinated to this cation site are of two nonequivalent types ($O_b$ and $O_{nb}$) and calculations were performed where each of these was moved from their respective lattice sites before the relaxation was begun. Ionic relaxation of both these two starting geometries resulted in the same converged structure with an increase in the Li−$O_{nb}$ distance from 1.86 to 1.89 Å (Figure 3). This is a smaller increase than for the (110) and (100) surfaces, which may be due to the lack of an oxygen ion in the site opposite the extended Li−O bond that would provide a Coulombic interaction reinforcing bond extension.

For the O-terminated (111) surface, there are two possible Mg lattice sites at which the Li-dopant can be introduced (i.e., the bridging and the nonbridging sites). Calculations were performed on the two configurations, and for both configurations elongation of one Li−O distance was found with Li−O distances of 2.19 Å (from 1.88 Å in the pure surface) and 1.89 Å (from 1.86 Å in the pure surface) for the bridging and nonbridging dopant sites, respectively. The relaxed structure of the nonbridging $[Li'_{Mg}O^{\bullet}_{O}]$ defect on the oxygen-terminated (111) surface is shown in Figure 4.

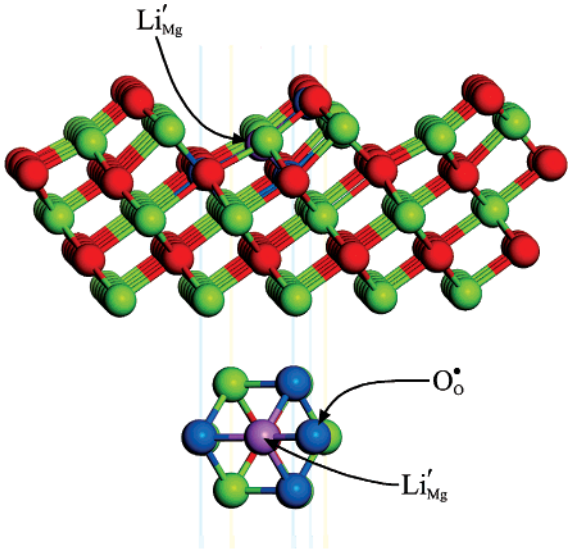


**Figure 4.** The relaxed geometry of the Li-doped (111) O-terminated MgO surface with $[Li'_{Mg}O^{\bullet}_{O}]$ defect (shown for the nonbridging Li-dopant). Side view (upper panel) and top view (lower panel) of the geometry around the Li-dopant.

To examine the effect of the presence of a $[Li'_{Mg}O^{\bullet}_{O}]$ defect on the electronic structure, the partial (ion and angular momentum decomposed) electronic density of states (PEDOS) were calculated by projecting the wavefunctions onto spherical harmonics centered on the ions, with radii of 1.40 Å for Mg, 1.50 Å for O, and 1.40 Å for Li. These radii are consistent with charge density plots of the valence electron density and result in the correct number of valence electrons for such a projection. Figure 5a−d shows the spin-polarized O 2p PEDOS for the O ion with the elongated Li−O distance for the (100), (110), (111) Mg-terminated and (111) O termination (bridging oxygen). The energy is plotted relative to the top of the valence band. A narrow peak is present 5 eV below the valence band edge for the (100), (110), and Mg-terminated (111) surfaces, which arises from population of the O 2p state with a single electron. A wide band of states extends from 4.5 eV below the valence band up to the valence band edge. For the O-terminated (111) surface, the lower energy peak is coupled with this main O 2p valence band. Finally, an unoccupied gap state is found 1.0 eV (100), 1.4 eV (110), 1.9 eV Mg-terminated (111) and 1.4 eV O-terminated (111) above the valence band and below the onset of the conduction band. This gap state arises from the O 2p hole trapped on the oxygen ion and is a consequence of the +1 charge Li-dopant replacing a Mg ion with a formal charge of +2.

To clarify the nature of the gap state identified from the PEDOS, the partial electron density was calculated for the region of the EDOS around the gap states in each surface. A density slice is shown for the (100), (110), and (111) Mg-terminated and (111) O-terminated (nonbridging) in Figure 6a−d. For each system, the excess spin is of O 2p character and is strongly localized on a single $O^{-}$ ion, the oxygen ion with the Li−O interatomic distance extended relative to the corresponding MgO bond length in the stoichiometric surface. Both terminations of the (111) surface exhibited the same characteristics in the electron density. The PEDOS and partial electron density maps together clearly demonstrate the existence of a localized

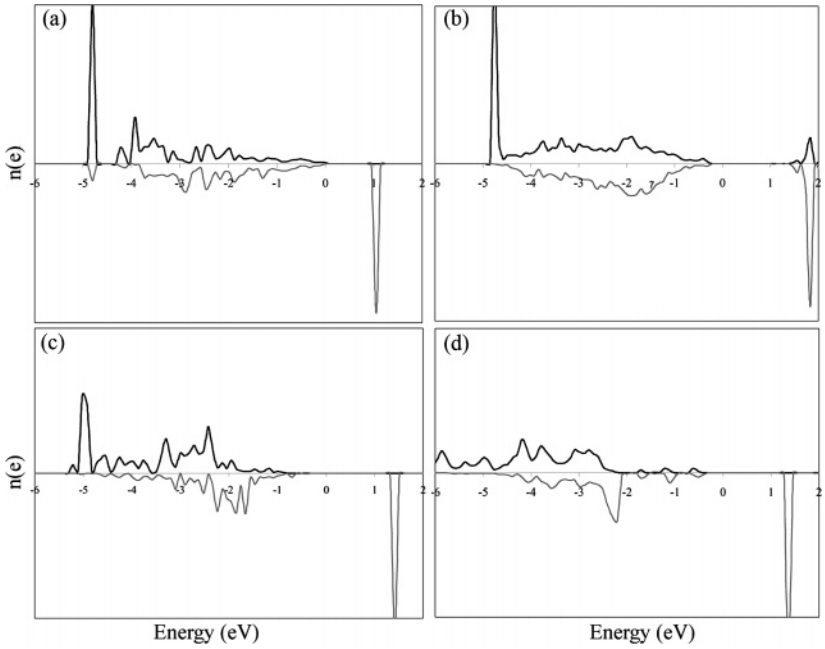


**Figure 5.** O 2p PEDOS for Li-doped MgO surfaces with $[Li'_{Mg}O^{\bullet}_{O}]$ defect (black spin up, gray spin down). (a) (100) termination, (b) (110) termination, (c) (111) Mg termination, and (d) (111) O termination (bridging oxygen).

electronic hole state on O in each of the low index surfaces of MgO. This illustrates that DFT+*U*, as employed in this study, can accurately describe the electronic effects of this Li-defect on different MgO surfaces.

The energy of formation associated with the $[Li'_{Mg}O^{\bullet}_{O}]$ defect on each surface can be calculated according to the following equation:

$$MgO_{slab} + Li_2O + (1/2)O_2 \rightarrow MgO(2[Li - O])_{slab} + 2MgO$$

The calculated formation energies are listed in Table 1 with DFT+*U* applied to oxygen in all systems. It should be noted that these formation energies have not been corrected for the well-documented errors in the DFT-calculated binding energy of O2.[44−47] In standard DFT, this error normally overstabilizes $O_2$ by as much as 0.7 eV with reference to experiment.[48] However, comparison with the experimental value[49] indicates that the error when using DFT+*U* is only of the order of 0.1 eV.

The formation of the $[Li'_{Mg}O^{\bullet}_{O}]$ oxygen hole defect on MgO is energetically favorable (negative formation energies) for the (110) and (111) surface terminations. For the more stable (100) surface, the cost of forming the defect is 0.51 eV $Li^{-1}$.

**3.3. Lithium-Doping with Oxygen Vacancy Formation.** To form a $[Li'_{Mg}\ V^{\bullet\bullet}_{O}\ Li'_{Mg}]$ defect, two magnesium surface atoms are each replaced with lithium in a clustered configuration, and a single neighboring oxygen atom is removed to form an oxygen vacancy. Two different oxygen vacancy configurations were considered for the (100) Li-doped surface, both of which are shown in Figure 7. In the first arrangement, the two Li ions are in a linear configuration with the oxygen vacancy in between them (labeled $\alpha_{100}$) and with all three sites lying in the surface (100) plane. In the second configuration, the two Li ions are positioned so that the vacancy forms a 90° angle between them (type $\beta_{100}$) again with all three sites in the surface plane. The relaxed geometries for both configurations are displayed in Figure 7a,b. In both cases, ionic relaxation results in all surrounding cations moving away from the vacancy site.

Three different oxygen vacancy configurations were explored for the doped (110) MgO surface. The first (type $\alpha_{110}$) has both Li ions on one ridge of the surface with the oxygen vacancy directly between them in a colinear arrangement, as shown in Figure 8a. The second configuration (type $\beta_{110}$) consists of two Li ions sitting on adjacent ridges on the surface with the oxygen vacancy on the surface of the lower ridge between them, forming a 90° Li−V−Li angle, Figure 8b. In the third configuration (type $\gamma_{110}$), one Li ion sits in a Mg site on a ridge and the second is in an adjacent Mg site in one of the two neighboring lower Mg−O−Mg rows. The oxygen vacancy is again on an upper ridge forming a 90° Li−V−Li angle, Figure 8c. In all cases, ionic relaxations resulted in the neighboring cations moving away from the vacant oxygen lattice site with the smaller singly charged Li substituents moving further off their lattice sites than the unsubstituted Mg ions.

A single oxygen vacancy configuration was calculated for the Mg-terminated (111) MgO surface, which is shown in Figure 9a. The two Li-dopants lie in the same exposed uppermost row of ions with the oxygen vacancy in a bridging lattice site in the adjacent subsurface row of five-coordinate oxygens. Relaxation of the structure resulted in the distortion of the Li ions away from their substitutional positions. The resulting Li−O interatomic distances for each Li ion are reduced to 1.83 and 1.70 Å.

For the oxygen-terminated (111) surface, two different vacancy configurations were considered. In both cases, the vacancy site was a surface-terminating oxygen site. Such sites have three neighboring cation sites, two bridging and one nonbridging, and two of which are substituted by Li in creating the vacancy. This gives one possible structure where the two Li atoms occupy the nonbridging site and one of the (equivalent) bridging sites, $Li_b-V-Li_{nb}$, and another structure where both the bridging sites are substituted, $Li_b-V-Li_b$. The first of these gives a relaxed structure with the two Li ions distorted away from their initial positions and drawn toward the bulk, Figure 9b, with Li−O interatomic distances of 1.91 and 2.02 Å. The second configuration shows similar distortions upon relaxation with Li−O interatomic distances of 1.83 Å (Figure 9c).

The valence electron density isosurfaces for the oxygen vacancy configurations on the (100) surface are shown in Figure

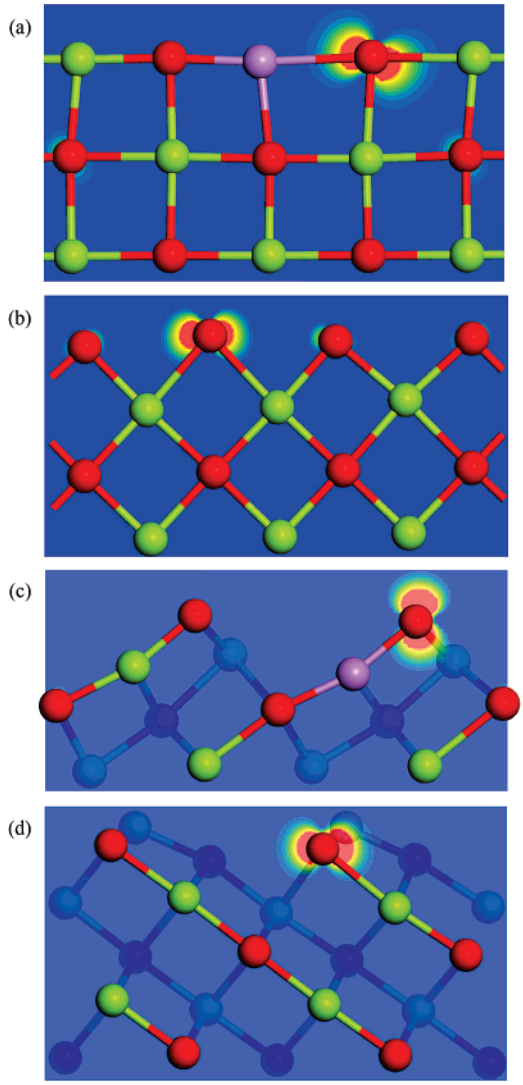


**Figure 6.** Side view of the partial electron density around the defect state in Li-doped MgO with [$Li'_{Mg}O^{\bullet}_{O}$] defect on the (a) (100) surface, (b) (110) surface and (111) (c) O-terminated, and (d) Mg-terminated surfaces. The density shows localization on the oxygen atoms neighboring the Li-dopant. The contour map is shown for from 0 (blue) to 0.4 electrons $Å^{-1}$ (red).

7c,d. Accumulation of charge density is not observed in the vacancy positions on each of these surfaces, indicating that this defect does not result in a localized charge on the oxygen ions, in contrast with the observations made for the [$Li'_{Mg}O^{\bullet}_{O}$] defect center. The vacancy sites for the other surface terminations are similarly found to have an absence of charge density.

The calculated EDOS were examined for each of the vacancy structures. No defect gap states were found, and this absence of a compensating electronic hole state is consistent with the charge density plots.

The energies of formation of the [$Li'_{Mg}$ $V^{\bullet\bullet}_{O}$ $Li'_{Mg}$] defect centers were calculated according to

$$MgO_{slab} + 2Li_2O \rightarrow MgO(2[2Li + O_{vac}])_{slab} + 4MgO$$

The energies for each surface are listed in Table 2. For the (100) surface, the two vacancy configurations ($\alpha_{100}$ and $\beta_{100}$) are isoenergetic with formation energies of +0.65 eV per Li atom. For the (110) surface, the formation energies for the three configurations are −0.99 eV (type $\alpha_{110}$), +0.52 eV (type $\beta_{110}$), and −0.27 eV (type $\gamma_{110}$), indicating that oxygen vacancy

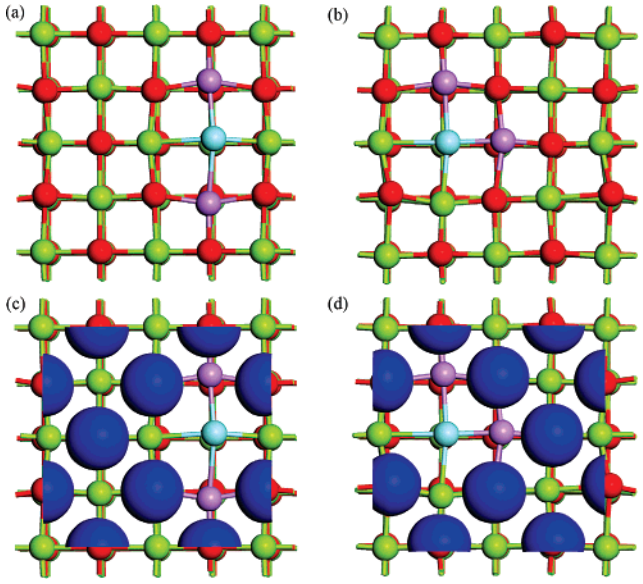


**Figure 7.** Top views for (a) Type $\alpha_{100}$ and (b) Type $\beta_{100}$ [$Li'_{Mg}$ $V^{\bullet\bullet}_{O}Li'_{Mg}$] defect configurations in the (100) Li-doped surface of MgO. The oxygen vacancy position is indicated schematically by a blue atom. The resulting charge densities are shown in (c) and (d), respectively, for the surface layer. The isosurface (blue) is shown for 0.15 electrons $Å^{-1}$.

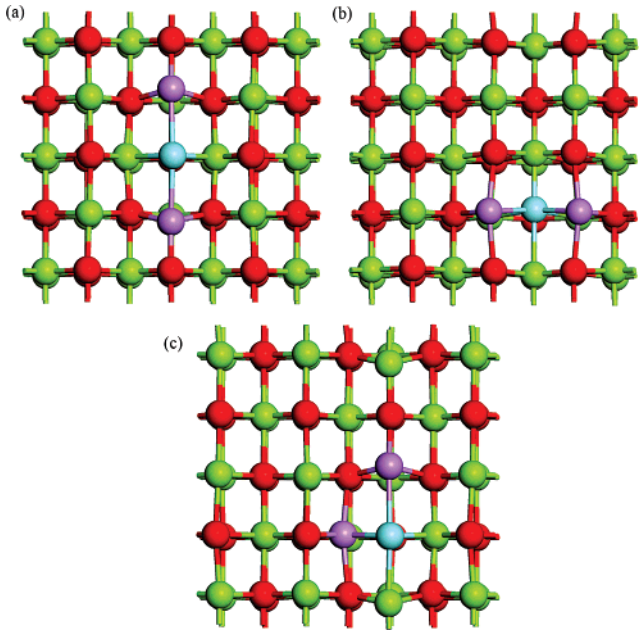


**Figure 8.** Top views of the three [$Li'_{Mg}$ $V^{\bullet\bullet}_{O}$ $Li'_{Mg}$] defect configurations for Li-doped (110) MgO: (a) $\alpha_{100}$, (b) $\beta_{110}$, and (c) $\gamma_{110}$. The oxygen vacancy position is indicated schematically by a blue atom.

formation is more stable in the outermost layer with the ordering of energies as might be expected from electrostatic considerations. For the Mg-terminated (111) surface, the vacancy formation energy is −0.70 eV, while for the O-terminated (111) surface, the formation energy is −1.36 eV for one Li in a bridging site and the other in the nonbridging site. The alternative (111) O-terminated vacancy (both Li atoms in bridging sites) has a formation energy of −0.73 eV. Substitution by a Li atom at a bridging five-coordinate Mg site is energetically unfavorable compared with alternative substitution at a nonbridging four-coordinate site.

**3.4. Lithium-Doping with Lithium Interstitials.** Li-doping of the surfaces of MgO with additional lithium interstitials to

**TABLE 1: Energy of Formation for the [$Li'_{Mg}O^{\bullet}_{O}$] Defect on the Low Index Surfaces of MgO**

| surface | energy of formation (eV per Li) |
|---|---|
| (100) | +0.51 |
| (110) | −1.58 |
| Mg-terminated (111) | −2.04 |
| O-terminated (111) - $Li_{nb}$ | −2.06 |
| O-terminated (111) - $Li_{b}$ | −1.08 |

produce a [$Li'_{Mg}Li^{\bullet}_{i}$] defect have also been considered, and the resulting structures are shown in Figure 10a−c. For the (100) surface, the interstitial lithium is coordinated to a single oxygen atom and the substituted Li atom (Figure 10a). The interstitial Li in the (110) surface is bridging between two surface oxygen atoms (Figure 10b). For the Mg-terminated (111) surface, the interstitial Li in a [$Li'_{Mg}Li^{\bullet}_{i}$] defect is coordinated to three oxygen ions (Figure 10c). Such surface interstitial sites would be occupied by surface Mg atoms in a non-reconstructed MgO (111) surface, and it is therefore unsurprising that they provide stable sites for an additional interstitial cation when the surface has been reconstructed to give (100) microfacetting. The corresponding sites for the O-terminated (111) surface would be occupied by O atoms in a non-reconstructed surface, and each vacant site has three neighboring Mg cations. It is therefore electrostatically unfavorable for these sites on the (100) microfacetted surface to be occupied by an interstitial Li cation, and no attempt was made to model what would be a very high-energy configuration. Examination of the electron density and density of states confirmed the absence of any defect state in the band gap, as expected due to the presence of two Li atoms.

The energy of formation for the [$Li'_{Mg}Li^{\bullet}_{i}$] defect can be calculated using the equation

$$MgO_{slab} + 2Li_2O \rightarrow MgO(2[2Li])_{slab} + 2MgO$$

The formation energies for each surface are shown in Table 3. Generation of the [$Li'_{Mg}Li^{\bullet}_{i}$] defect is only unfavorable on the (100) surface with a formation energy of +0.51 eV $Li^{-1}$. The (110) and Mg-terminated (111) surfaces result in energies of −0.59 and −1.06 eV $Li^{-1}$ respectively.

## 4. Discussion

For the three surfaces considered, the effect of Li-doping with oxygen hole electronic compensation on the geometry and electronic structure is qualitatively the same. All doping positions show an elongation of a single Li−O interatomic distance, although the precise length of the extended bond varies between surfaces. For example, for the (100)-terminated MgO surface the Li−O distance is 2.37 Å, while it is 1.89 Å for the (111) surface. All the [$Li'_{Mg}O^{\bullet}_{O}$] defect centers display the same features in the electronic structure: localization of the electronic hole on a single oxygen site (the oxygen ion involved in the elongated Li−O distances) and the appearance of a new feature in the electronic density of states, lying between the valence band and the conduction band. Thus, we have demonstrated that formation of a (potentially) catalytically active defect center through substitutional Li-doping is possible on each of the low index surfaces.

The formation of the [$Li'_{Mg}V^{\bullet\bullet}_{O}Li'_{Mg}$] defect center also produces similar results on each surface. For all the configurations considered, there are no electrons present in the vacancy site and no gap state is observed in the EDOS. The absence of charge in the vacancy site indicates these defect centers are likely to be catalytically inactive, a result which is independent of the choice of surface.

The formation of the [$Li'_{Mg}Li^{\bullet}_{i}$] defect center also displayed results that are again qualitatively the same for the three surfaces. The calculated EDOS do not contain any gap states, and no excess or localized charge is found in the equilibrium charge density. This indicates the formation of another defect center, which is likely to be catalytically inactive; this is a result that is independent of the choice of surface.

Differences between the surfaces are found when the formation energies of these defects are considered. For the stable low energy (100) surface, all three types of Li-doping are energetically unfavorable. Of the three defect types considered, Li-doping of the surface with oxygen hole electronic compensation and Li interstitials are by far the most energetically accessible defects with formation energies of +0.51 and +0.50 eV per Li-dopant, respectively. In comparison, the formation energy of an oxygen vacancy on the Li-doped surface is +0.65 eV $Li^{-1}$. However, in a low oxygen partial pressure environment the formation of an oxygen vacancy will be more favored.

For the (110) and (111) surface terminations, very different results are found. For the (110) surface, there are negative formation energies for the three Li-defect centers. This indicates that either defect center could readily form on this surface. Of the different defects and configurations considered, the isolated [$Li'_{Mg}O^{\bullet}_{O}$] defect is the most energetically favorable (−1.58 eV per Li) with the linear oxygen vacancy configuration ($\alpha_{110}$) also highly favored (−0.99 eV). The only unfavorable defect configuration is the $\beta_{110}$ oxygen vacancy where the oxygen vacancy is between the Li-dopants but is situated in the plane of a lower surface ridge in a fully coordinated lattice site. For the Mg (111)-terminated surface, the formation of each defect type is also energetically favorable. The isolated [$Li'_{Mg}O^{\bullet}_{O}$] defect has a formation energy of −2.04 eV, while the oxygen vacancy and lithium interstitial defects result in a defect again of −0.70 eV and −1.06 per Li-dopant, respectively.

Similar results are found for the O-terminated (111) surface where the formation of the defect centers are again energetically favored over the stoichiometric MgO surface. The nonbridging [$Li'_{Mg}O^{\bullet}_{O}$] defect results in an energy gain of −2.06 eV, while the [$Li'_{Mg}V^{\bullet\bullet}_{O}Li'_{Mg}$] defect results in the formation energy of −1.36 eV $Li^{-1}$. The alternative oxygen vacancy with lithium substituents in both the bridging sites has a slightly less favorable formation energy of −0.73 eV. This difference is because substituting at a four-coordinate-nonbridging site causes a smaller penalty to the Madelung energy than doing so at a five-coordinate-bridging site, as seen above in the energetics of the [$Li'_{Mg}O^{\bullet}_{O}$] O-terminated (111) surface.

The strong surface dependence for the Li-doping of MgO is of consequence for catalytic reactions. The interaction of a hydrogen atom with the Li-defect site on the surface of Li-doped MgO is currently considered as the most likely mechanism for the catalytic coupling of methane. A C−H bond of methane is cleaved with the resulting hydrogen bonding to the surface $O^{-}$ site produced by the Li-dopant. This DFT+*U* study suggests that of the defect centers considered, isolated [$Li'_{Mg}O^{\bullet}_{O}$] defects are energetically favorable on the (110)- and (111)-terminated surfaces. However, on both these surfaces the formation of oxygen vacancies and Li interstitials upon Li clustering are also energetically favorable and thus will show dependence on oxygen partial pressure. With a high dopant concentration, it is therefore possible that defect centers will be adopted that do not contain an active $O^{-}$ site, hence, reducing the catalytic activity of the material. This corresponds qualitatively to

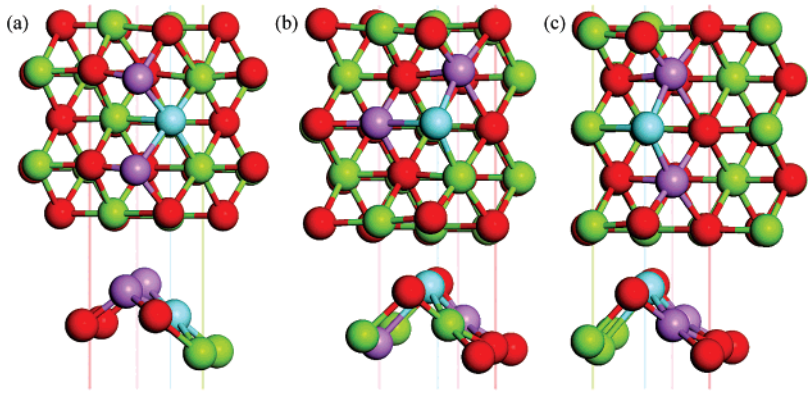


**Figure 9.** The relaxed geometry of the $[Li'_{Mg}V^{\bullet\bullet}_{O}Li'_{Mg}]$ defect on (a) the (111) Li-doped Mg-terminated, (b) the $Li_b-O-Li_{nb}$ configuration on the (111) O-terminated surface, and (c) the $Li_b-O-Li_b$ configuration on the (111) O-terminated surface. The oxygen vacancy position is indicated schematically by a blue atom.

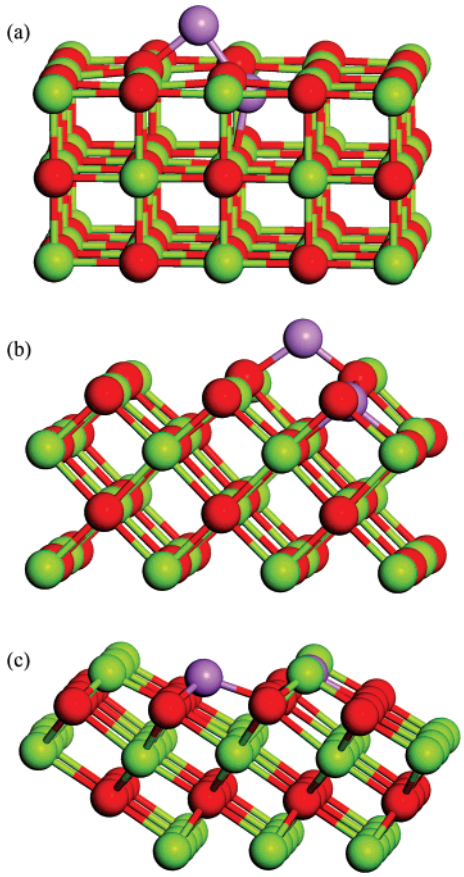


**Figure 10.** The relaxed geometry of the $[Li'_{Mg}Li_i^{\bullet}]$ defect for (a) (100) surface, (b) (110) surface, and (c) (111) Mg-terminated surface.

**TABLE 2: Energy of Formation for the $[Li'_{Mg}\ V^{\bullet\bullet}_{O}Li'_{Mg}]$ Defect on the Low Index Surfaces of MgO**

| surface | energy of formation (eV per Li) |
|---|---|
| (100) | +0.65 ($\alpha_{100,}\beta_{100}$) |
| (110) | −0.99 ($\alpha_{110}$) |
| | +0.52 ($\beta_{110}$) |
| | −0.27 ($\gamma_{110}$) |
| Mg-terminated (111) | −0.70 |
| O-terminated (111) | −1.36 |
| | −0.73 (both Li bridging) |

experimental evidence that increasing the Li-dopant concentration above 7% leads to a reduction in the catalytic activity of Li-doped MgO.[48]

**TABLE 3: Energy of Formation for the $[Li'_{Mg}Li_i^{\bullet}]$ Defect on the Low Index Surfaces of MgO**

| surface | energy of formation (eV per Li) |
|---|---|
| (100) | +0.50 |
| (110) | −0.59 |
| Mg-terminated (111) | −1.06 |

## 5. Conclusions

In this study, we have used DFT+*U* to investigate the defect centers in Li-doped MgO on the low index (100), (110), and (111) surfaces. We have investigated structural, electronic, and energetic features of the defect centers formed through isolated Li-doping with electronic compensation (the formation of catalytically active oxygen hole states) and through clustering of pairs of Li atoms accompanied by oxygen vacancy formation or Li interstitials.

On the three surfaces, Li-doping with electronic compensation results in a distortion of the geometry around the dopant site with strong elongation of a single Li−O distance. This oxygen atom is found to carry the electronic hole that results from the doping process, and a new electronic state appears between the valence band and the conduction band in agreement with experiment.

To examine the possible mechanism for Li-doping on each of the low index surfaces, we have computed defect energies of formation for each of the Li-defect centers. We find a very strong surface dependence. On the (100) surface, while all the defects considered cost energy to form, Li-doping with oxygen hole electronic compensation or Li interstitials are favored relative to oxygen vacancy formation on the doped surface. Conversely, the formation of an oxygen vacancy is favored on the doped (110) surface. Importantly, the formation of each defect configuration results in a substantial energy gain over the stoichiometric surface. As such, either defect could be expected to form readily. On both terminations of the (111) surface, energy gains are also observed for formation of each defect center. Isolated Li-doping with oxygen hole formation is the most energetically favored defect for the Mg-terminated surface, and vacancy formation is the most favored for the O-terminated surface.

The results presented in this paper follow from a detailed examination of the surface dependence of formation of defect centers in Li-doped MgO as well as an understanding of the relative stability of active and inactive defect centers. This provides a foundation for a complete description of the catalytic coupling of methane on doped metal oxide surfaces.

**Acknowledgment.** We acknowledge support for this work from Science Foundation Ireland (Grant Numbers 04/BR/C0216 and 05/RFP/CHE0035) and the HEA for the IITAC PRTLI (Cycle III) grant. All calculations were performed on the IITAC supercomputer, as maintained by TCHPC. We would also like to thank P.M. Oliver and S.C. Parker for numerous useful discussions over many years.

## References and Notes

(1) Ito, T.; Lunsford, J. H. *Nature* **1985**, *314*, 721.
(2) Lunsford, J. H. In *Methane Conversion by Oxidative Processes*; Wolf, E. H., Ed.; Van Nostrand Reinhold: New York, 1992.
(3) Wu, M. C.; Truong, C. M.; Goodman, D. W. *Phys. Rev. B* **1992**, *46*, 12688.
(4) Tover, H. T.; Abraham, M. M.; Chen, Y.; Henderson, B. *Phys. Rev. B* **1972**, *5*, 3276.
(5) Abraham, M. M.; Unruh, W. P.; Chen, Y. *Phys. Rev. B* **1974**, *10*, 3540.
(6) Abraham, M. M.; Chen, Y.; Boatner, L. A.; Reynolds, R. W. *Phys. Rev. Lett.* **1976**, *37*, 849.
(7) Chen, Y.; Tover, H. T.; Narayan, J.; Abraham, M. M. *Phys. Rev. B* **1977**, *16*, 5535.
(8) Lacy, J. B.; Abraham, M. M.; Boldú, O. J. L.; Chen, Y.; Narayan, J.; Tohver, H. T. *Phys. Rev. B* **1978**, *18*, 4136.
(9) Hutchings, G. J.; Scurrell, M. S.; Woodhouse, J. R. *J. Chem. Soc., Chem. Comm.* **1989**, *12*, 765.
(10) Cant, N. W.; Lukey, C. A.; Nelson, P. F.; Tyler, R. J. *J. Chem. Soc., Chem. Comm.* **1989**, *12*, 766.
(11) Driscoll, D. J .; Martir, W.; Wang, J. X.; Lunsford, J. H. *J. Am. Chem. Soc.* **1985**, *107*, 58.
(12) Zuo, J.; Pandey, R.; Kunz, A. B. *Phys. Rev. B* **1991**, *44*, 7187.
(13) Lintuluoto, M.; Nakamura, Y. *J. Mol. Struct.* **2004**, *674*, 207.
(14) Lachinot, A.; Larrieu, C.; Zicoovich-Wilson, C.; Roetti, C.; Orlando, R.; Dovesi, R. *J. Phys. Chem. Solids* **1998**, *59*, 1119.
(15) Lachinot, A.; Larrieu, C.; Orlando, R.; Dovesi, R. *J. Phys. Chem. Solids* **1998**, *59*, 7.
(16) Dovesi, R.; Orlando, R.; Roetti, C.; Pisani, C.; Saunders, V. R. *Phys. Status Solidi B* **2000**, *217*, 63.
(17) Yang, Z. X.; Liu, G.; Wu, R. Q. *Phys. Rev. B* **2002**, *65*, 235432.
(18) Dash, L. K.; Gillan, M. J. *Surf. Sci.* **2004**, *549*, 217.
(19) Nolan, M.; Watson, G. W. *Surf. Sci.* **2005**, *586*, 25.
(20) Laegsgaard, J.; Stokbro, K. *Phys. Rev. B* **2002**, *11*, 075208.
(21) McMahan, A. K.; Martin, R. M.; Satpathy, S. *Phys. Rev. B* **1988**, *38*, 6650.
(22) Potze, R. H.; Sawatzky, G. A.; Abbate, M. *Phys. Rev. B* **1995**, *51*, 11501.
(23) Chainani, A.; Mathew, M.; Sarma, D. D. *Phys. Rev. B* **1992**, *46*, 9976.
(24) Nolan, M.; Watson, G. W. *J. Chem. Phys.* **2006**, *125*, 144701.
(25) D' Avezac, M.; Calandra, M.; Mauri, F. *Phys. Rev. B* **2005**, *71*, 205210.
(26) Chainani, A.; Mathew, M.; Sarma, D. D. *Phys. Rev. B* **1993**, *48*, 14818.
(27) Ackermann, L.; Gale, J. D.; Catlow, C. R. A. *J. Phys. Chem. B* **1997**, *101*, 10028.
(28) Dudarev, S. L.; Botton, G. A.; Savrasov, S. Y.; Humphreys, C. J.; Sutton, A. P. *Phys. Rev. B* **1998**, *57*, 1505.
(29) Shick, A. B.; Pickett, W. E.; Liechtenstein, A. I. *J. Electron Spectrosc. Relat. Phenom.* **2001**, *114*, 753.
(30) Anisimov, V. I.; Zaanen, J.; Anderson, O. K. *Phys. Rev. B* **1991**, *44*, 943.
(31) Kresse, G.; Hafner, J. *Phys. Rev. B* **1994**, *49*, 14251.
(32) Kresse, G.; Furthmuller, J. *Comput. Mater. Sci.* **1996**, *6*, 15.
(33) Blöchl, P. E. *Phys. Rev. B* **1994**, *50*, 17953.
(34) Perdew, J.; Burke, K.; Ernzerhof, M. *Phys. Rev. Lett.* **1994**, *77*, 3865.
(35) Nolan, M.; Grigoleit, S.; Parker, S. C.; Sayle, D. C.; Watson, G. W. *Surf. Sci.* **2005**, *576*, 217.
(36) Nolan, M.; Parker, S. C.; Watson, G. W. *Phys. Chem. Chem. Phys.* **2006**, *8*, 216.
(37) Murnaghan, F. D. *Proc. Nat. Acad. Sci. U.S.A.* **1944**, *30*, 244.
(38) Watson, G. W.; Kelsey, E. T.; de Leeuw, N. H.; Harris, D. J.; Parker, S. C. *J. Chem. Soc., Faraday Trans.* **1996**, *92*, 433.
(39) Tasker, P. W. *J. Phys. C: Solid State Phys.* **1979**, *12*, 4977.
(40) Oliver, P. M.; Parker, S. C.; Mackrodt, W. C. *Modell. Simul. Mater. Sci. Eng.* **1993**, *1*, 755.
(41) Wander, A.; Bush, I. J.; Harrison, N. M. *Phys. Rev. B* **2003**, *68*, 233405.
(42) Broqvist, P.; Gronbeck, H.; Panas, I. *Surf. Sci.* **2004**, *554*, 262.
(43) Robach, O.; Renaud, G.; Barber, A. *Surf. Sci.* **1998**, *401*, 227.
(44) Johnson, B. G.; Gill, P. M. W.; Pople, J. A. *J. Chem. Phys.* **1993**, *98*, 5612.
(45) Curtiss, L. A.; Raghavachari, K.; Redfern, P. C. *J. Chem. Phys.* **1997**, *106*, 1063.
(46) Hammer, B.; Hansen, L. B.; Nørskov, J. *Phys. Rev. B* **1999**, *59*, 7413.
(47) Nolan, M.; Parker, S. C.; Watson, G. W. *Surf. Sci.* **2005**, *595*, 223.
(48) *CRC Handbook of Chemistry and Physics*, 67th ed.; Weast, R. C., Ed.; CRC Press: Boca Raton, FL, 1987.
(49) Peng, X. D.; Richards, D. A.; Stair, P. C. *J. Catal.* **1990**, *12*, 99.